In Vivo Chronic Brain Cortex Signal Recording Based on a Soft Conductive Hydrogel Biointerface

In Vivo Chronic Brain Cortex Signal Recording Based on a Soft Conductive Hydrogel Biointerface

*Chiara Rinoldi, Yasamin Ziai, Shahrooz Zargarian, Paweł Nakielski, Krzysztof Zembrzycki, Roberto Fiorelli, Massimiliano Lanzi, Agnieszka Kostrzewska-Księżyk, Rafał Czajkowski, Ewa Kublik, Leszek Kaczmarek, Filippo Pierini**

Dr. C. Rinoldi, Y. Ziai, Dr. S. Zargarian, Dr. P. Nakielski, K. Zembrzycki, Dr. R. Fiorelli, Prof. F. Pierini

Department of Biosystems and Soft Matter and Laboratory of Polymers and Biomaterials, Institute of Fundamental Technological Research, Polish Academy of Sciences, Warsaw 02-106, Poland

E-mail: fpierini@ippt.pan.pl

Prof. M. Lanzi
Department of Industrial Chemistry "Toso Montanari", Alma Mater Studiorum University of Bologna, Bologna 40136, Italy

A. Kostrzewska-Księżyk, Dr. R. Czajkowski, Dr. E. Kublik, Prof. Leszek Kaczmarek
Nencki Institute of Experimental Biology Polish Academy of Sciences, Warsaw 02-093, Poland

Keywords: nanocomposites, conductive hydrogels, neural interface recording, neuroinflammation, in vivo mouse model.

Commentato [1]: up to 7

The acquisition of neural signals from the brain cortex has always been crucial in the field of neuroscience to analyze brain processes and individuate neurological disorders. Nowadays, the design of a neural interface conformable to the brain tissue is one of the major challenges, since the insufficient biocompatibility of those systems provokes fibrotic encapsulation response, leading to inaccurate signal recording and potential misdiagnosis. Herein, the design and production of a novel soft neural biointerface composed of polyacrylamide hydrogels loaded with plasmonic silver nanocubes are reported. The nanostructured hydrogels are surrounded by a silicon-based template as a supporting element for guaranteeing a tight neural-hydrogel contact, while allowing a stable recording from specific locations of the

cortex. The nanostructured hydrogels show superior conductivity properties, while mimicking the brain tissue's mechanical characteristics. Furthermore, *in vitro* biological tests performed by seeding neural progenitor cells demonstrate the biocompatibility of the hydrogel-based system as well as neuronal differentiation. *In vivo* long-term neuroinflammation tests on a mouse model report no adverse immune response toward the nanostructured hydrogel-based neural interface. Additionally, electrocorticography acquisitions demonstrate that the proposed platform permits a long-term efficient recording of neural signals, revealing the suitability of the system as a chronic neural biointerface.

1. Introduction

The acquisition of neural signals from the brain cortex has always been of high relevance in the field of neuroscience.[1] Moreover, extending electrophysiological recording/stimulation in the brain cortex from days to years may help understand brain processes and neurological diseases and disorders.[2,3] Electrocorticography (ECoG) stimulation can improve spatial specificity compared to electroencephalography (EEG) electrodes since the stimulation electrodes are placed directly on the cortical surface.[4,5] ECoG is beneficial in monitoring epilepsy for presurgical planning and is a therapeutic tool to reduce seizures or neuropathic pain.[5] Moreover, due to the high signal-to-noise ratio and a localized cortical signal, it can be used for neuroprosthetic research to provide sensory feedback of external devices in the brain-computer interface (BCI).[6] However, conventional subdural or epidural electrodes can exhibit immune responses that lead to fibrous encapsulation of the probe due to the chemo-mechanical mismatch between the probes and the neural tissue[7]. Conventional solid-state interfaces are not explicitly designed to fit the complex mechanical properties of tissues and may injure soft tissues.[5] Most importantly, inadequate conformability with the brain cortex might lead to inaccurate signal recording and potential misdiagnosis[8]. Ongoing efforts to mitigate this problem should include developing deformable and conformable materials with favorable electrical properties.[2]

Hydrogels have gained increased attention as interfaces between biological and engineered systems due to their tissue-like mechanical properties.[9] They are a promising candidate for neural interfaces since they exhibit very low Young's modulus (~kPa) compared with thermoplastics and elastomers (~MPa) or gold and platinum (~GPa). Moreover, due to their high water content, the soluble ions can quickly move in the absorbed water, thus enabling ionic conduction.[10] In addition, heat generated during current injection dissipates in a water-rich hydrogel which prevents local burns and pain in the case of traditional electrodes placed

directly on the cortical surface.[10] Furthermore, the hydrophilicity of a hydrogel matrix also prevents the adsorption of proinflammatory proteins onto the electrode surface.[5] The prevention of biofouling results from the strong binding of water molecules to the surface of the hydrogel and hence a higher energetic cost of surface dehydration.

Several hydrogel formulations have been explored as neural probe coatings or standalone.[11–13] However, due to hydrogels' poor intrinsic ionic conductivity, other approaches need to be undertaken to increase their conductivity.[11] Nanostructured hydrogels constitute a combination of nanotechnology and biomaterial science that can improve electrical properties. The hydrogel matrices have been loaded with conductive materials such as metallic fillers (e.g., nanowires, nanoflakes, or micro-, nano-particles), and carbon-based conductive materials (e.g., nanotubes or graphene) to form a percolation network within a hydrogel matrix.[14–17] One of the advantages of this approach includes signal transmission by the transfer of ions and small molecules, similarly to human biological tissues.[2] Thus, the tissues have much higher electrical conductivity than using electrons and holes as the charge carriers in metal electronic devices.

In this research, we design and produce a soft neural biointerface composed of polyacrylamide (PAAm) hydrogel loaded with plasmonic silver nanocubes (AgNCs) to provide the system with good electrical properties. The nanostructured hydrogel is surrounded by a template of two layers of silicon-based materials (i.e. polydimethylsiloxane (PDMS) and soft skin adhesive) as supporting elements for guaranteeing a tight and stable neural-hydrogel contact while allowing a stable signal acquisition from specific locations of the brain cortex for an extended period. An electrically conductive hydrogel composite that has a low electrical impedance (<3 kΩ at 10Hz) and Young's modulus (<10 kPa) that matches soft tissues like neural tissue. The flexible electrode can be well fitted on the brain surface and can shake synchronously with the weak movement of the brain, which supplies a powerful safeguard to avoid tissue harm during brain micro-movement, thus providing compliance with nerve tissue and allowing a stable long-term neural recording.

2. Results and Discussion

In order to design a material for neural signal acquisition, it is of key importance to develop a biocompatible conducting platform capable of transmitting the neural signals, while guaranteeing the matching of brain mechanical properties for creating a stable recording interface. In this work, we propose a soft neural biointerface based on nanostructured hydrogels made of PAAm with the addition of AgNCs, in order to provide the system with

good electrical properties. To achieve the final formulation, acrylamide (AAm) is dissolved in deionized water in presence of N,N'-methylene bisacrylamide (BIS-Aam), and photoinitiator (Irgacure 2959). AgNCs are added to the solution in a concentration of 20% wt/wt$_{monomer}$, forming the hydrogel precursor. Afterward, the solution is bubbled with argon to remove all the oxygen molecules and then exposed to UV light to allow the PAAm/AgNCs hydrogel crosslinking.

Six PAAm/AgNCs nanostructured hydrogels with a diameter of 1 mm are then placed in dedicated holes created by punching two layers of silicon-based material in relevant locations for in vivo animal signal acquisition. The first layer is made of soft skin adhesive to properly adhere to the brain skull, thus permitting a stable contact for the recording of neural cortex signals. The second layer is composed of PDMS to protect the neural acquisition system from adhesion to the mouse head skin after closing the surgery site and for handling reasons. Finally, the hydrogel-based neural biointerface is located on the mouse skull where relevant holes have been drilled in order to reach the brain cortex in correspondence to the hydrogel location to record specific neural cortex signals upon amplifying, filtering, digitizing and feeding the signals to a personal computer (**Figure 1**).

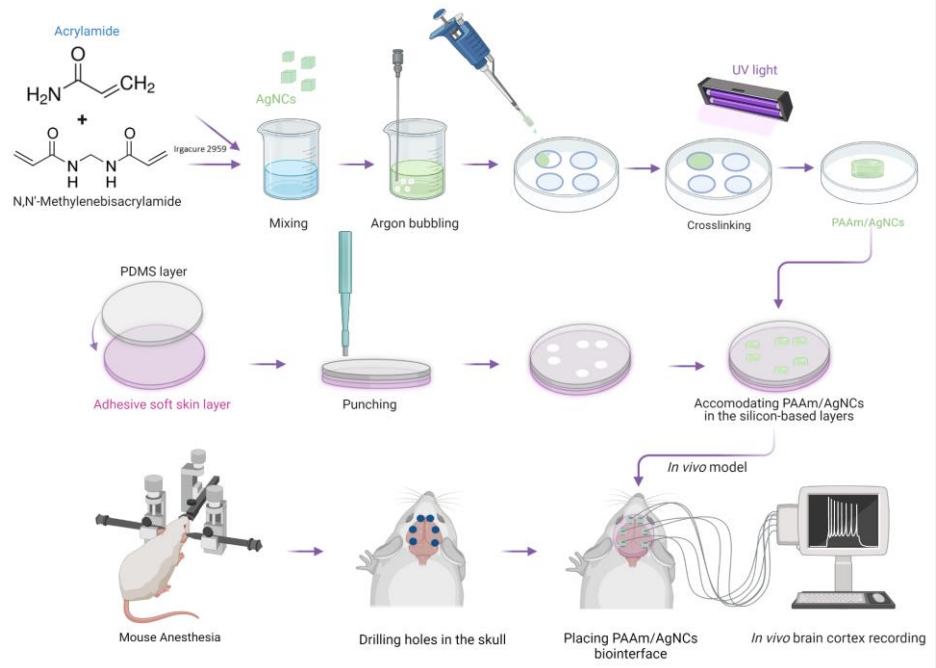

Figure 1. Fabrication and application scheme of the hydrogel-based biointerface. The hydrogel solution is prepared by dissolving AAm, BIS-Aam, and photoinitiator in deionized water. AgNCs are then added to the hydrogel precursor, and the solution is bubbled with argon and then exposed to UV light for permitting the PAAm/AgNCs hydrogel crosslinking. Later, six hydrogels are located in dedicated holes created by punching two layers of silicon-based material (i.e. soft skin adhesive and PDMS). The final system is then placed on the mouse skull where relevant holes have been drilled to reach the brain cortex and allow for specific signals acquisition on a personal computer.

Figure 2 represents the morphology, size distribution, and spectroscopy properties of AgNCs utilized in this study to be embedded into the PAAm hydrogel. As shown in the field emission scanning electron microscopy (FE-SEM) images in Figure 2a (displayed at two different magnification levels), AgNCs are well dispersed and have an average dimension of 100 nm. AgNCs are in a perfect cubic form with distinctive visible edges and corners.
As can be seen from the Transmission Electron Microscopy (TEM) image shown in Figure 2b-c, the AgNCs have a regular and well-defined cubic shape with sharp edges. The homogeneous distribution of AgNCs in an aqueous environment, their high colloidal stability, and a significantly low degree of agglomeration in the absence of a dispersion medium are proved. It is visible that the silver nanocubes have a single population. The corresponding energy-dispersive X-ray spectroscopy (EDX) analysis is represented in Figure 2d, confirming the elemental composition. The silver element distributes uniformly throughout the whole cubic area of AgNCs and matches well with the measures calculated from the TEM image. AgNCs particle size and distribution profile in suspension was determined using the DLS technique. The method then correlates the hydrodynamic radius of the nanomaterials in their colloidal dispersion to hypothetical spherical particles having a similar rheological behavior as the object under study. The latter can then be translated into the particle size and size distribution.[18] The average hydrodynamic particle size of AgNCs has measured ~109 nm in diameter (Figure 2e). The DLS pattern also reveals that AgNCs are monodisperse, with a narrow distribution, in the range of 98 to 119 nm. Studying DLS in combination with TEM provides the advantage of confirming the modality of nanoparticles and accurate assessment of their hydrodynamic diameter. The consistency between the observed and calculated data acquired from FE-SEM, TEM, and DLS point to high colloidal stability, regularity, and homogeneity of the AgNCs and promises a good dispersion of these nanocubes in the aqueous

environment, which will be further used as the precursor solution for the preparation of PAAm/AgNCs hydrogel.

UV-vis was used to observe the absorption spectra of the AgNCs (Figure 2f). The excitation of surface plasmon vibration of the silver nanocubes changed the color of the suspension, and a pronounced absorbance peak at $\lambda = 505$ nm was recorded. The peak at the mentioned wavelength and the overall profile of the absorption spectra are typical for silver nanoparticles with cubic shapes.

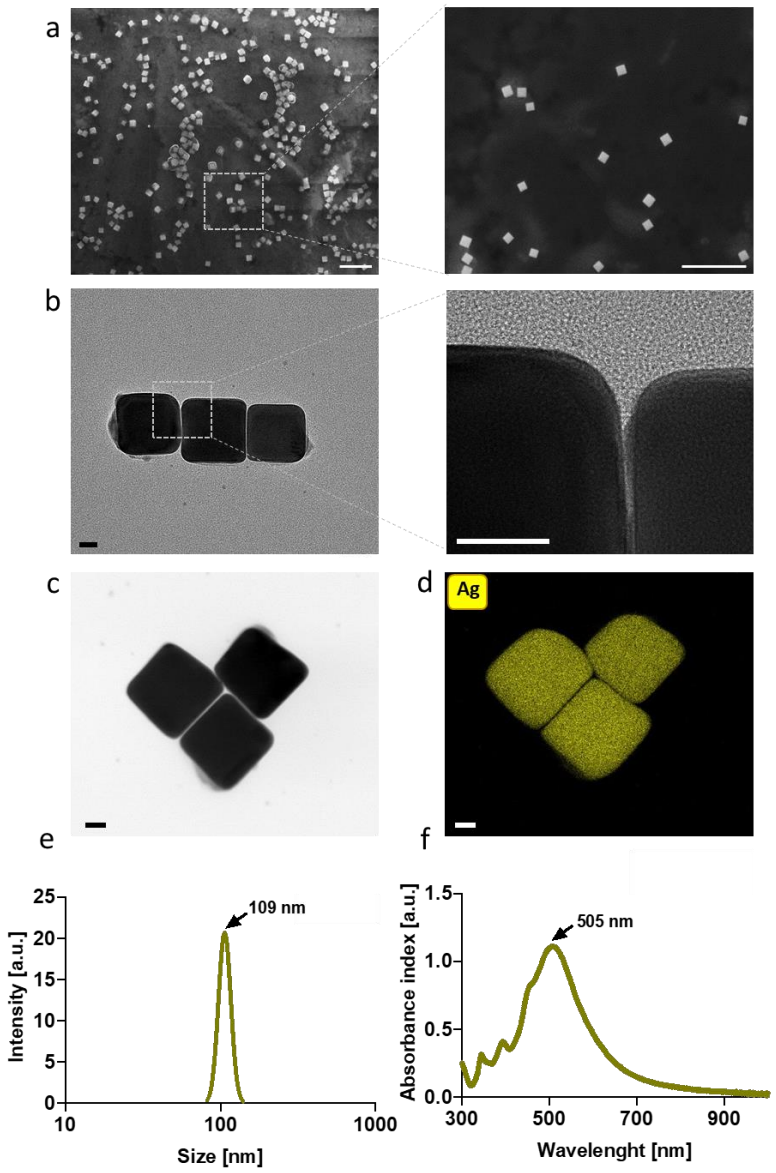

Figure 2. Characterization of AgNCs: a) FE-SEM images, showing the cubic shape and morphology of the nanocubes. The cube's size is measured at around 100 nm. Scale bars: 500 nm; b-c) TEM micrographs, displaying the shape and well-defined edges of the silver nanocubes. Scale bar: 20 nm; d) EDX images, confirming the uniform silver elemental composition of the nanocubes. Scale bar: 20 nm; e) DLS graph, highlighting the narrow distribution of the cube size in the range of 98 to 119 nm, with an average diameter of 109

nm; f) UV-Vis graph, reporting an absorbance peak at λ = 505 nm typical for cubic silver nanoparticles.

Polyacrylamide (PAAm) is a well-known polymer that has attracted much attention in various fields of bio-nanotechnology due to its several interesting physicochemical properties.[19,20] PAAm hydrogels are homogeneous, stable hydrophilic polymeric gels with high optical transparency and chemical robustness.[21] They are biocompatible and non-resorbable with antifouling properties that prevent cell and nonspecific protein adsorption.

Figure 3a represents the FE-SEM images of the lyophilized PAAm and PAAm/AgNCs hydrogels. The pristine PAAm hydrogel shows a 3D uniform microporous structure. The average pore size of this cell-like network is 68 μm. The interconnected porous cell-like structure remains intact with the introduction of silver nanocubes; however, the average pore size increases slightly to 77 μm. Therefore, it can be assumed that AgNCs did not disrupt the UV-initiated radical polymerization of acrylamide monomers and the simultaneous crosslinking process. While silver-containing hydrogel shows fewer wrinkles and a fairly more ordered microporous structure, the appearance of pore wall ripples for both samples under study is similar, proving the formation of a highly stable suspension of AgNCs in the PAAm matrix and their distribution in the pore walls of microporous PAAm/AgNCs hydrogel. Moreover, the favorable hydrodynamic condition of our system may result in the self-assembly of AgNCs, guiding the formation of ripples with a smooth surface (as it can be visualized after the lyophilization process). This assumption can be cross-checked for validation by investigating the topography of the proposed samples (Figure 3b). Indeed, it can be observed that the presence of silver nanocubes on the surface of PAAm/AgNCs hydrogel is negligible. As also evidenced by high-resolution TEM and corresponding EDX images (Figure 3c,d), AgNCs result trapped and well dispersed within the hydrogel network. The chemical composition of PAAm/AgNCs is reported by Fourier transform infrared (FT-IR) spectroscopy measurements (**Figure S1**). Comparing the spectra obtained for PAAm pristine hydrogel vs PAAm/AgNCs, it is possible to visualize the presence of the main functional groups related to the presence of PAAm in the hydrogel network. On the other hand, AgNCs quantity into the final structure might be not sufficient to be detected by the instrument.

A scanning electron microscopy image of the cross-section of the hydrogel network embedded with AgNCs is reported in Figure 3e. The micrograph represents the final layered structure, in which PAAm/AgNCs hydrogels are placed in holes created into two silicon-based layers. The porous 3D structure retains its uniformity after the cutting procedure, and

the cell-like network is still visible in the cross-sectional image. The image displays the detail of the PAAm/AgNCs hydrogel in contact with the PDMS layer, where a robust interface between the two structures promises a compact and easy-to-handle neural recording platform. The mechanical properties of PAAm hydrogels can be modulated by changing the ratio of monomers to crosslinkers before polymerization in order to reach values that can match the mechanical features of the target tissue application. In this study, the ratio of acrylamide to BIS-Aam concentration was optimized at 5.26% w/w in order to attain sufficient mechanical properties to recapitulate the mechanical characteristics of the brain tissue. Acrylate-based hydrogels have a high swelling ratio and retain remarkable amounts of water that lead to a crucial decrease in their physical strength and cause their ease breaking. For these reasons, the application of polymeric hydrogels presents several limitations. The development of nanostructured hydrogels, upon introduction of nanoparticles into a hydrogel network, can promote and sustain the mechanical integrity of the hydrogel, while improving its toughness and strength. In this study, the effect of AgNCs embedded into the PAAm hydrogel on the mechanical properties can be detected via a comparison of Young's Modulus of the neat hydrogel vs. PAAm/AgNCs (Figure 3f). The nanoindentation graph reveals that AgNCs incorporated hydrogel showed significantly higher mechanical strength than their pristine counterpart. More specifically, Young's Modulus values of ~1.9034 +/- 0.183154 kPa and ~7.599 +/− 0.651398 kPa were detected for the designed PAAm and PAAm/AgNCs hydrogels, respectively, successfully matching the mechanical properties of brain tissue slice (1–10 kPa). Since the mechanical strength of PAAm/AgNCs mimics well the mechanical characteristics of the brain tissue, enhanced stability of the interface between the developed silver–incorporated PAAm hydrogel and the brain cortex is expected. The remarkable four–fold increase in PAAm/AgNCs Young's Modulus compared to that of PAAm hydrogel can be associated with several factors such as newly formed polymer/particle-polymer/polymer interactions, higher crosslinking density, and self-assembly of nanoparticles. Indeed, Qin et al. recently showed that the in situ self-assembly of nanoparticles creates a new network in the gel structure, leading to its physical crosslinking, and significantly improving the mechanical properties of nanostructured hydrogel.[22] The authors argued that the exceptional mobility of short polymeric chains, which for instance, are

attached to the surface of a nanoparticle, may contribute to the self-assembly of the nanophase in the matrix.

Finally, incorporating nanoparticles into the structure can provide functional properties such as electroconductivity for hydrogels. As discussed previously, in situ polymerization of acrylamide in the presence of silver nanocubes favors a regular distribution and dispersion of the particle during polymer crosslinking, allowing the formation of a composite network with uniform properties. On the other hand, the self-assembly of AgNCs may form ordered contacts and efficient conductive channels. Hence, the results of the electrical test, performed on PAAm/AgNCs and PAAm hydrogels, demonstrate a significantly lower electrical impedance of silver incorporated hydrogel at the entire range of frequency ($1–10^5$ Hz, **Figure S2**). Figure 3g represents the electrical impedance results at 10 Hz, a relevant frequency for biomedical applications. As seen, the impedance of PAAm hydrogel is 6.51 +/- 1.03 kΩ, which is 2.57 folds higher than the value reported in the case of PAAm/AgNCs. Moreover, 2.43 folds higher values of surface electrical conductivity were recorded for the PAAm/AgNCs hydrogel compared to PAAm hydrogel. These measurements are promising for enhancing the conduction of neural electrical signals via the hydrogel platform embedded with silver nanocubes. Overall, the uniform dispersion of the silver nanocubes into the network of PAAm/AgNCs interconnected porous structure and the formation of conductive channels, significantly contribute to the improved electroconductive property of the system for the ultimate application of the material.

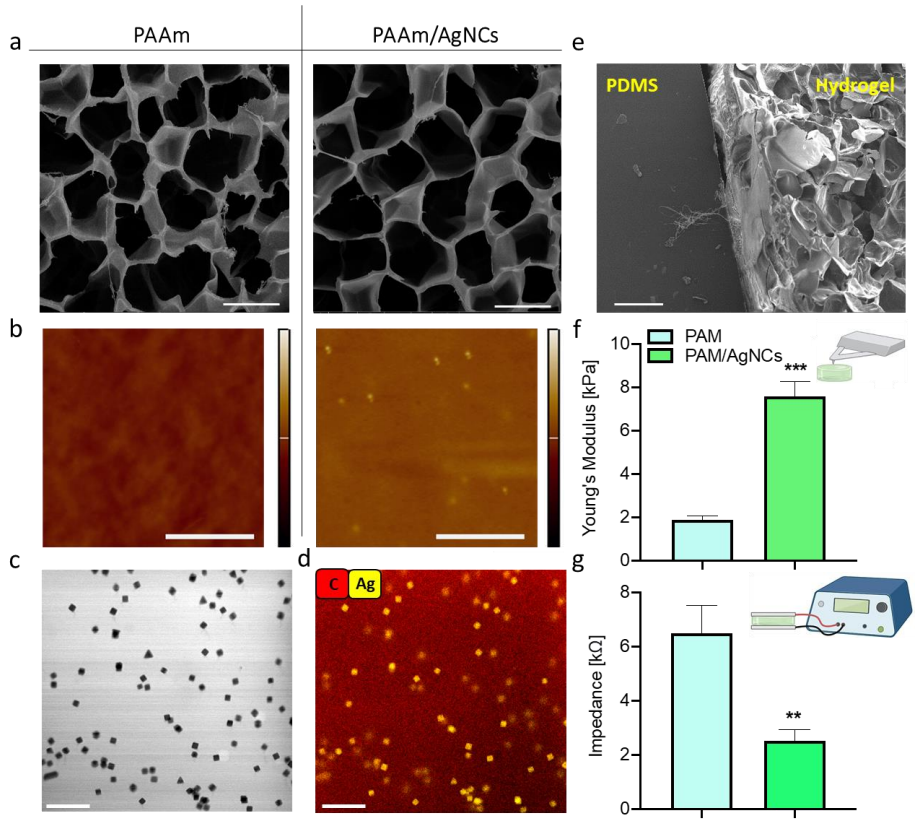

Figure 3. Morphological and physical characterization of the hydrogel systems. a) FE-SEM images of PAAm hydrogel compared to PAAm/AgNCs hydrogel, showing the 3D uniform interconnected microporous structure. Scale bars: 10 um; b) AFM micrographs of PAAm hydrogel compared to PAAm/AgNCs hydrogel, displaying the topography of the samples. Scale bar: 2 µm, Z scale bar: 110 nm (PAAM), 60 nm (PAAm/AgNCs). c) TEM micrograph of PAAm/AgNCs hydrogel, highlighting that AgNCs are embedded and well dispersed within the hydrogel network. Scale bars: 500 nm. d) EDX image of PAAm/AgNCs hydrogel, highlighting the chemical composition of the nanoscructured hydrogel. Scale bars: 500 nm. e) SEM image of the cross-section of the final layered structure, evidencing the robust and compact interface between the PAAm/AgNCs hydrogel and the PDMS layer. Scale bar: 100 um. f) Young's Modulus histogram, reporting the mechanical properties of PAAm/AgNCs compared to PAAm hydrogels detected through the nanoindentation method. g) Histogram of the electrical impendence values detected at physiological relevant frequency (10 Hz),

showing the superior electrical properties of PAAm/AgNCs hydrogel. Significant differences are shown as: *p < 0.05, **p < 0.01, ***p < 0.001.

As aforementioned, the biocompatibility of the system is a crucial aspect since the material is expected to be implanted in contact with the brain cortex for several weeks with no adverse reactions. To demonstrate the *in vitro* compatibility of PAAM and PAAm/AgNCs hydrogels to the neural tissue, the response of neural progenitor cells (NPCs) in contact with the materials was evaluated. More in detail, the isolation of NPCs from the sub-ventricular zone of postnatal mouse brains was carried out upon brain extraction. The dissected sub-ventricular zone tissue was digested, and NPCs were filtered and cultured in an incubator at 37°C and 5% CO_2. After cell expansion, mature floating neurospheres were seeded on PAAm and PAAm/AgNCs hydrogels to evaluate their biocompatibility and specific neural response in terms of differentiation into neural and glial cells (**Figure 4**a-c). In **Figure S3** it is possible to visualize that, after cell seeding, the neurospheres adhered to the tested hydrogels. During the culture time, NPCs migrated in the radial direction from the center of the neurosphere, expressing specific neural markers (MAP2, green color) and astrocyte markers (GFAP, red color), thus creating a differentiated cellular network.

The expression of specific markers reveals the phenotype of cells seeded on the hydrogel substrates. More specifically, the immunohistochemistry staining of relevant neural markers (MAP2 and GFAP) during the culture time is reported in **Figure 5**, while image analysis to quantify the cellular differentiation into neural and glial cells up to 10 days is shown in Figure 4b,c. Results show a trend of significantly higher expression of MAP2 in the case of NPCs seeded on PAAm/AgNCs compared to PAAm hydrogel at each time point selected during the culture time (Figure 4b). Additionally, the quantity of MP2-positive neurons increases up to 10 days of culture in the case of PAAm/AgNCs substrate, while it does not experience a significant enhancement on PAAm hydrogel. On the other hand, the expression of GFAP is measured as comparable for pristine and hydrogel composites during the cell culture time (Figure 4c). Increasing GFAP-positive astrocyte expression over the culture time is observed in both cultures with no significant difference between the tested hydrogels.

Data reveal that the conductive nanostructured hydrogel PAAm/AgNCs is biocompatible and allow NPCs survival, attachment, and spreading while supporting neuronal differentiation.

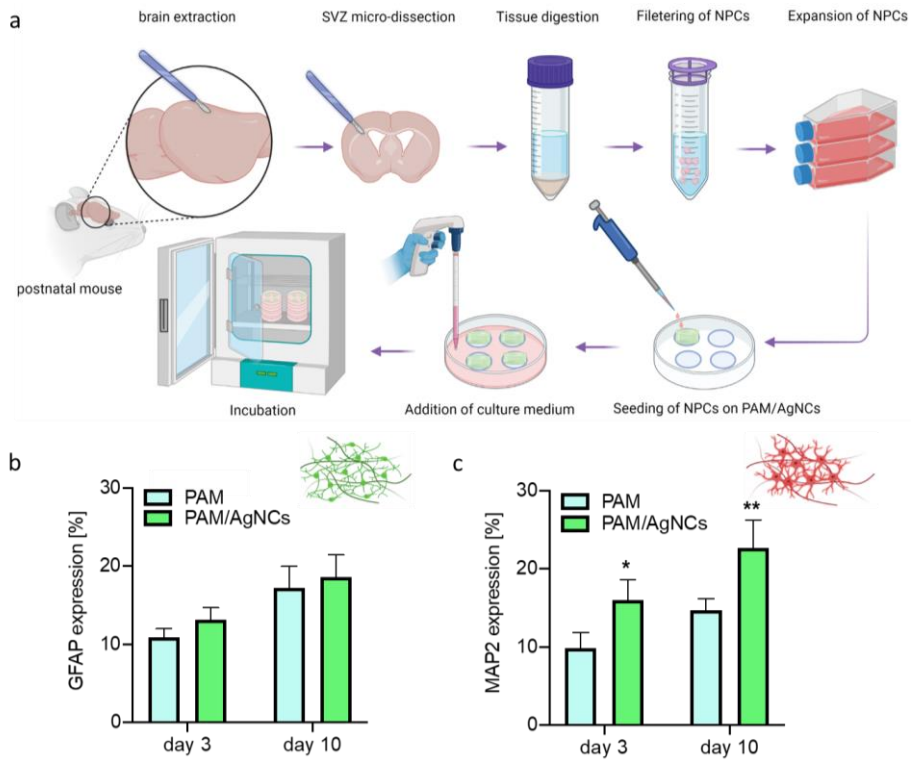

Figure 4. Biological response of NPCs seeded onto PAAm and PAAm/AgNCs hydrogels. a) NPCs isolation and seeding – experiment schematic. The sub-ventricular zone of postnatal mouse brains is dissected, digested, and filtered to isolate NPCs. Cells are expanded in vitro, seeded onto the hydrogel substrates, and cultured in an incubator at 37°C and 5% CO_2. b) Quantification of Map2 expression in the immunostained images analyzed after 3 and 10 days of culture, showing a trend of significantly higher expression in the case of PAAm/AgNCs; c) Quantification of GFAP expression in the immunostained images analyzed after 3 and 10 days of culture, evidencing a comparable response in both substrates with no statistical difference. Significant differences are shown as: *$p < 0.05$, **$p < 0.01$, ***$p < 0.001$.

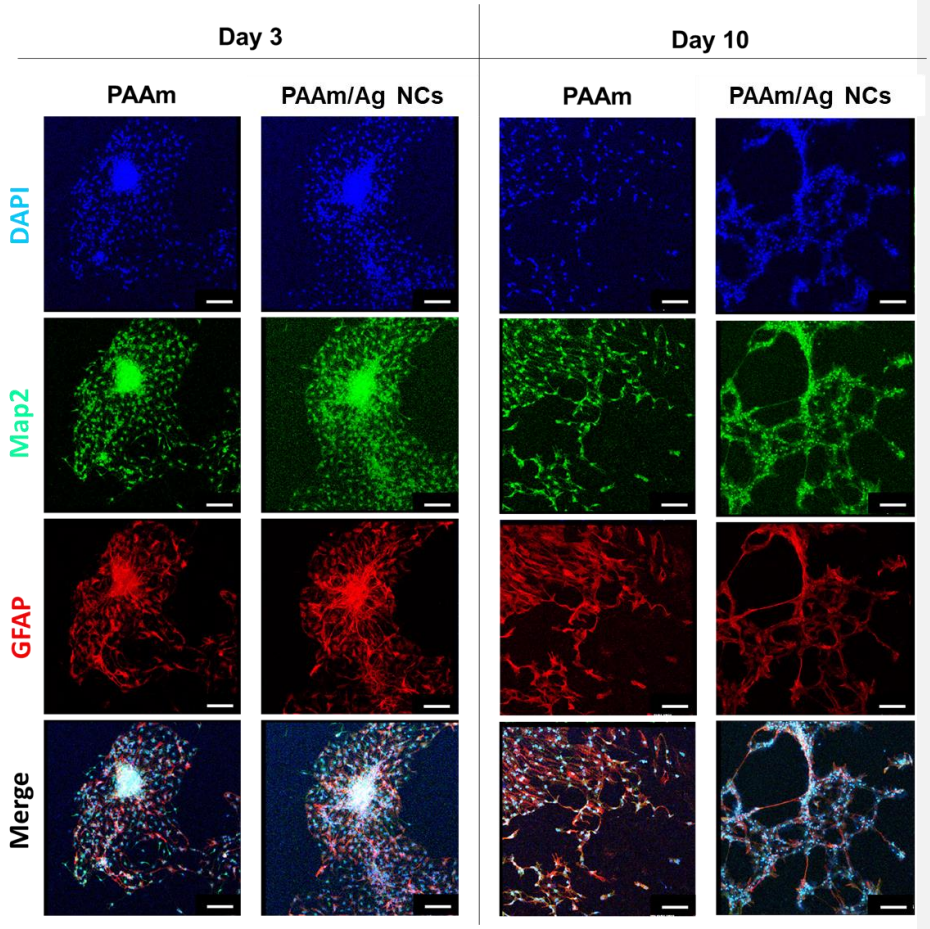

Figure 5. Immunohistochemical confocal images of NPCs cultured on PAAm and PAAm/AgNCs hydrogels after 3 and 10 days of culture. The expression of specific neuronal (MAP2), astrocytes (GFAP), and nuclei (DAPI) markers during the culture time can be visualized through the images. MAP2, GFAP expression, and DAPI stainings are reported in green, red, and blue colors, respectively. Scale bar: 100 µm.

Considering the promising biological properties of the system *in vitro*, biocompatibility *in vivo* was also assessed. PAAm/AgNCs- and PAAm-based hydrogels were implanted *in vivo* in a mouse model using protocols described previously [23,24]. Briefly, mice were anesthetized and their skull was thinned with a drill in four brain cortex regions where the hydrogels were placed. To evaluate the material's biocompatibility, the expression of three specific markers of

brain injury and inflammation were analyzed at 3 different time points up to 6 weeks post *in vivo* implantation.[25,26] Matrigel®, a well-established biocompatible material, was selected as the control condition. Non-treated regions were also analyzed. After harvesting the brains at 1 week, 3 weeks, and at 6 weeks, relevant marker of astrogliosis (GFAP), markers of microglia activation (Iba1, TMEM), and neuroinflammatory cytokine (TNF-alpha) were immunolabeled in the brain tissue areas adjacent to the implantation sites (**Figure 6**a-c). A significant upregulation of all the proteins is observed 1 week post-implantation (Figure 6d-f, **Figure S5**). Subsequently, the levels of GFAP, Iba1, and TNF-apha markers decline 3 weeks after surgery (**Figure S4**, 6d-f). In the case of GFAP, this trend continues also at the latest time point (6 weeks post-implantation), while the other markers remain stable. However, the expression of the selected relevant proteins outperforms the non-treated condition (indicated by the red line) in all the tested materials at each time point (except for TNF at late stage, Figure 6d-f, S5), thus confirming the transient immune response and the suitability of the systems for supporting microglia and astrocyte activities *in vivo*.

Additionally, no significant differences between PAAm/AgNCs hydrogel, PAAm hydrogel, and Matrigel are reported in the expression of any marker at any stage of the experiment. Hence, the results highlight the excellent biocompatibility of the PAAm/AgNCs hydrogel, revealing a weak *in vivo* immune response comparable to the Matrigel® condition, which is considered one of the best biomaterials in terms of biocompatibility since it is rich in extracellular matrix proteins.

For these reasons, considering its outstanding properties in terms of conductivity, mechanical properties, and biocompatibility, the proposed PAAm/AgNCs-based platform has been selected as a neural biointerface to proceed with the assessment of the ECoG experiment.

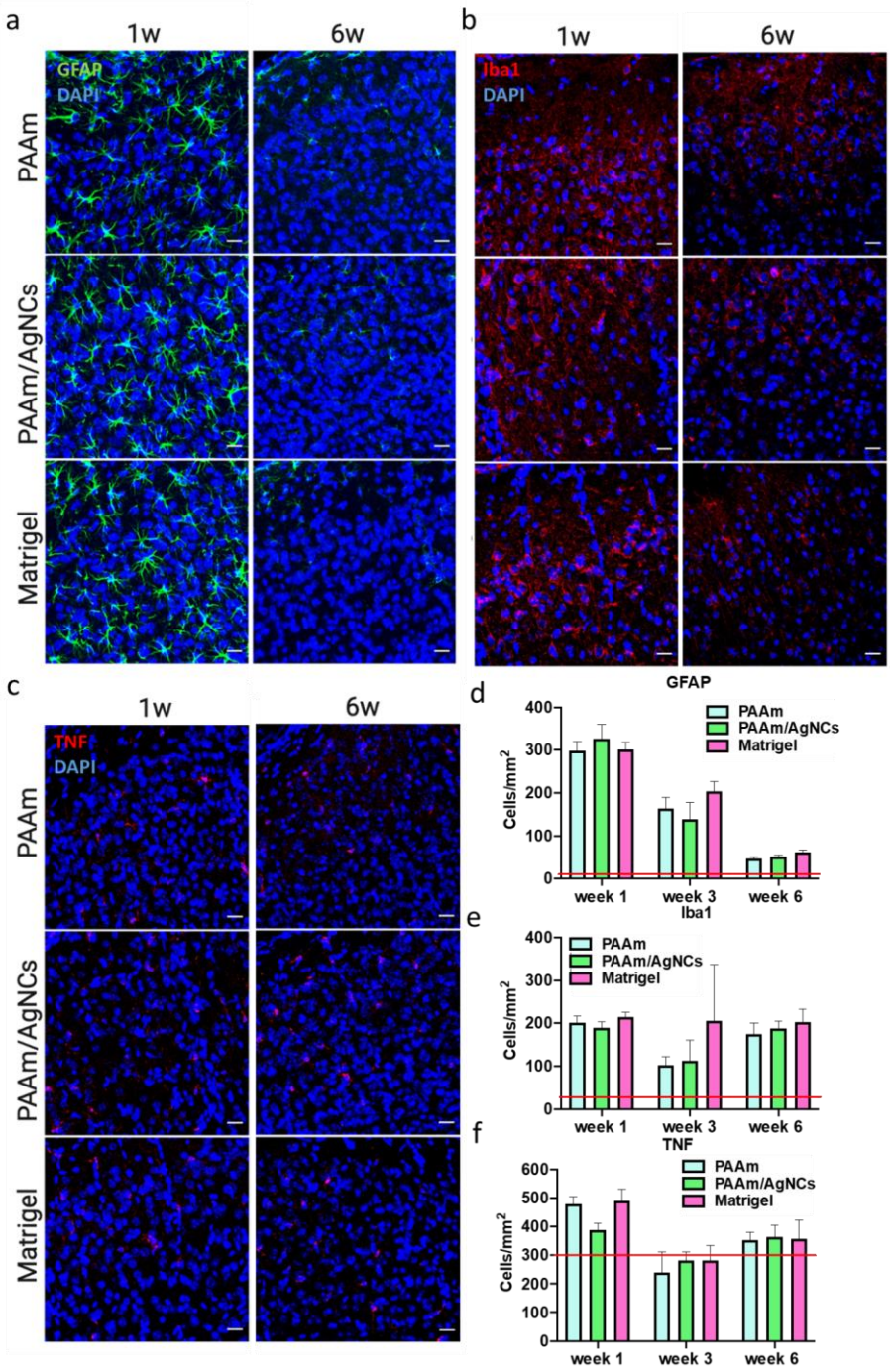
a
1w
6w
GFAP
DAPI
PAAm
PAAm/AgNCs
Matrigel
b
1w
6w
Iba1
DAPI
c
1w
6w
TNF
DAPI
PAAm
PAAm/AgNCs
Matrigel
d
GFAP
PAAm
PAAm/AgNCs
Matrigel
Cells/mm2
400
300
200
100
0
week 1
week 3
week 6
e
Iba1
PAAm
PAAm/AgNCs
Matrigel
Cells/mm2
400
300
200
100
0
week 1
week 3
week 6
f
TNF
PAAm
PAAm/AgNCs
Matrigel
Cells/mm2
600
500
400
300
200
100
0
week 1
week 3
week 6

Figure 6. *In vivo* biocompatibility of PAAm/AgNCs hydrogel, PAAm hydrogels, and Matrigel. Confocal images of immunostained brain sliced in contact with the materials for up to 6 weeks. Well-established neuroinflammation markers including GFAP (green color, a), Iba1 (red color, b), TNF (red color, c) are immunolabeled. Nuclei are stained with DAPI (blue color). Scale bars: 20 μm. The image quantification of GFAP (d), Iba1 (e), and TNF-alpha (f) is plotted in comparison with non-treated condition (red line), evidencing the outperformance of all tested materials at each time point (except for TNF al late stage).

Finally, the *in vivo* EcoG recordings were performed by anesthetizing the mice with isoflurane and subcutaneously injecting Tolfedine, Butomidor, and Baytril. Six specific locations on the brain skull were marked using stereotactic coordinates with reference to Bregma (2 in the frontal region of the brain cortex, 2 to the somatosensory regions, 2 to the visual regions). The skull was then drilled according to the selected locations and PAAm/AgNCs-based neural biointerface was placed gently on the surface (**Figure 7**a). *In vivo* signal acquisition was then performed by placing silver ball electrodes on the surface of tested materials. As a reference, the signals of the brain cortex were recorded by placing silver ball electrodes on its surface. Since the hydrogels had the tendency to dry when left exposed on the warm brain surface, for electrophysiological chronic recordings, electrodes were covered with an additional layer of soft medical-grade silicone which covered the scull and craniotomies and protected the hydrogels from drying (Figure 7a). ECoG signal was then amplified, filtered, digitized, and fed to a personal computer.

Somatosensory responses were evoked by the movement of the whiskers. Signals were instantaneously recorded through the implanted PAAm/AgNCs-based neural biointerface and compared to the activity of the brain cortex surface. In Figure 7b is possible to notice the successful acquisition of the signal by using the proposed platform with similar amplitudes to the reference signal. Chronic ECoG recordings show that after an initial decrease in amplitude at the first time point (i.e. 1 week post-surgery) - most probably due to the drying effect on the hydrogel materials - the acquired signal remains constant and the successful recording through the proposed neural biointerface is guaranteed up to 6 weeks after *in vivo* implantation (Figure 6c, **Figure S6**).

On the other hand, visual responses were evoked by a flash of diodes located 10 cm in front of the mouse's eyes. The same trend of signal acquisitions reported for the somatosensory evoked response is found also in the case of the visual evoked response. Indeed, acute recordings show comparable signals acquired through the PAAm/AgNCs-based neural

biointerface and the brain cortex surface (Figure 6d); while chronic signal acquisitions highlight the long-term efficiency of the system to acquire the brain cortex signals up to 6 weeks from surgery (Figure 6e, **Figure S7**).

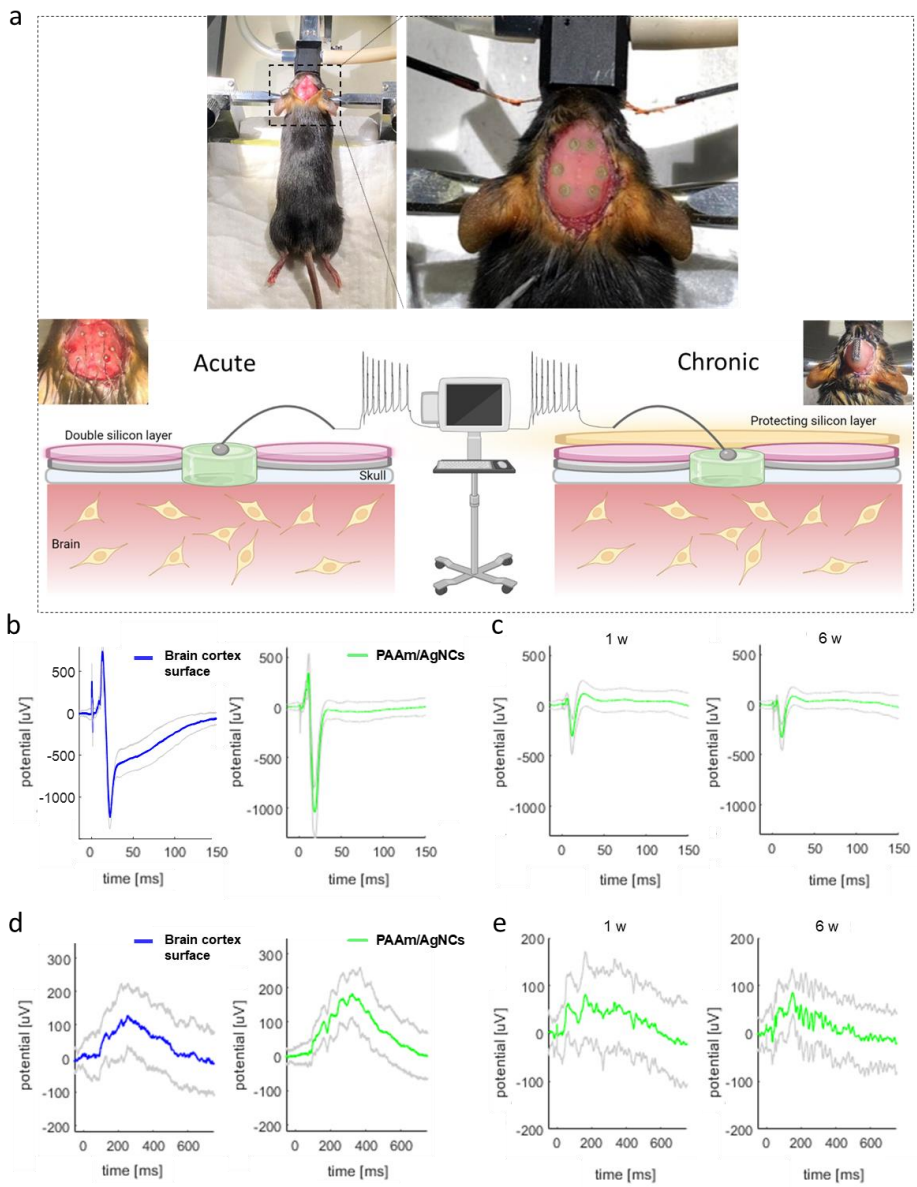

Figure 7. *In vivo* ECoG acquisition by using PAAm/AgNCs-based neural biointerface. a) Schematic representation of *in vivo* acute and chronic ECoG recordings. Six specific locations on the brain cortex were individuated using stereotactic coordinates with reference to Bregma. PAAm/AgNCs-based neural biointerface was placed on the brain tissue accordingly, in order to match the target recording regions. *In vivo* signal recording was carried out by placing silver ball electrodes on the surface of tested materials. In the case of chronic recordings, electrodes were covered with an additional layer of soft medical-grade silicone to prevent hydrogel drying. Finally, ECoG signal was fed to a personal computer. b) Acute somatosensory evoked potential response of PAAm/AgNCs-based neural biointerface compared to signals acquired from the brain cortex surface. c) Chronic somatosensory evoked potential response recorded through PAAm/AgNCs-based neural biointerface showing the successful long-term recording up to 6 weeks after implantation. d) Acute visual evoked potential response of PAAm/AgNCs-based neural biointerface compared to signals acquired from the brain cortex surface. e) Chronic visual evoked potential response of the PAAm/AgNCs-based neural biointerface, reporting efficient long-term signal acquisitions.

3. Conclusions

In this work, we design and successfully fabricate a soft, biocompatible neural biointerface composed of polyacrylamide hydrogel loaded with plasmonic silver nanocubes. The nanostructured hydrogels were collocated in dedicated holes created into a silicon-based template formed form of two layers of PDMS and soft skin adhesive, respectively. The silicon-based structure is designed as a supporting element in order to guarantee a tight and stable contact between the hydrogels and the brain tissue, thus allowing a tailorable and stable neural signal acquisition from specific locations selected on the cortex. The morphological, chemical, electrical, and mechanical properties of the platform are evaluated. The presence of AgNCs in the hydrogel polymeric structure leads to superior conductivity characteristics, while recapitulating the brain mechanical properties. Moreover, the investigation of neural progenitor cell response in contact with the proposed hydrogel demonstrates its biocompatibility *in vitro* and suitability for cell survival and neuronal differentiation. On the other hand, the *in vivo* biocompatibility of the system is proven through the evaluation of chronic neuroinflammation upon implantation in a mouse model. No adverse response is observed after brain slicing and staining for specific inflammatory markers (i.e. GFAP, Iba1, TNF-alpha, TMEM), revealing the weak immune response and the long-term in vivo biocompatibility of the proposed platform. Finally, *in vivo* ECoG recording conducted on a

mouse model reveal that the nanostructured hydrogel-based neural biointerface allows a successful long-term neural signal acquisition. Taking into account all the results, the biocompatible conductive nanostructured hydrogel-based device is a promising candidate as a neural biointerface for long-term brain signal acquisition without provoking neuroinflammation. The potential exploitation and translation of the proposed conductive hydrogel platform in electronic devices for human Electrophysiological Recording of Electrocorticographic or Electroencephalography Recording will be investigated in the near future.

4. Experimental Section

4.1. Materials

Acrylamide (AAm ≥ 99%, Sigma Aldrich, Poland), BIS−AAm (99.5%, Sigma Aldrich, Poland), 2−Hydroxy−4′−(2−hydroxyethoxy)−2−methylpropiophenone (Irgacure 2959, 98%, Sigma Aldrich, Poland), silver nanocubes (AgNCs, 75nm Silver nanocubes, PVP, Nanocomposix, USA), ammonium persulfate (APS, 98%, Sigma−Aldrich, Poland), *N*,*N*,*N*′,*N*′-tetramethylethylenediamine (TEMED, 99%, Sigma-Aldrich, Poland), Polydimethylsiloxane (PDMS, Sylgard 184 silicone elastomer kit), Soft skin adhesive (Liveo MG 7-9800) are used as received.

4.2. Design and fabrication of the PAAm/AgNCs-based neural biointerface

4.2.1. Preparation of the hydrogel precursor embedded with silver nanocubes

Hydrogel precursor sol is prepared by introducing 593.76 mg AAm as the base monomer and 31.25 mg BIS-AAm in the role of crosslinker; then, 12.5 mg of Irgacure 2959 is added as the photoinitiator. 10 ml of deionized water is added to the mixture, resulting in a 6.4 wt% solution. The solution is stirred overnight to reach complete dissolution while being wrapped in aluminum foil for light protection. An optimized concentration of silver nanocubes is determined in order to reach the highest concentration of AgNCs while preserving the hydrogel crosslinking process. More in detail, a suspension of AgNCs with 20% wt/$wt_{monomer}$ is added to the hydrogel precursor sol and stirred upon use. In the case of pristine hydrogel, the precursor solution is obtained following the same protocol except for AgNCs addition.

4.2.2. Production of the PAAm/AgNCs neural biointerface

The fabrication protocol of the final PAAm/AgNCs-based system provides first the preparation of the nanostructured hydrogel using photo-polymerization. The precursor sol is argon bubbled to evacuate all the oxygen molecules inside the solution to gain long-chain polymer networks via radical polymerization. In order to accelerate the polymerization, a very small amount of APS (2 μL mL−1) and TEMED (0.4 μL mL−1) are added to the final solution just before crosslinking. 100 μL of the solution was added to a 4-well Petri dish and was irradiated by UV light for 90 seconds.

On the other hand, PDMS and soft skin adhesive layers are prepared by mixing with a curing agent at a ratio of 10:1 wt % and 1:1 wt%, respectively, and degassed for 30 min. Afterward, 1mL of each solution was poured into a separated petri dish lid with a diameter of 35mm, to obtain ~ 1mm thick silicon-based layers. After complete crosslinking, the PDMS layer is placed on top of the soft skin adhesive layer, and the final system is punched with holes 1mm

in diameter. Prepared hydrogels are cut in the same dimension and accommodated into the pits to shape the final neural biointerface system.

4.3. Structural characterization

Morphological analysis of the hydrogel is performed to investigate the shape, size, and distribution of the AgNCs in an aqueous solution and inside the hydrogel structure.

SEM and FE-SEM are performed with JEOL JSM-6390LV and FEI Nova NanoSEM 450 microscopes, respectively. To obtain sharp cuts on the cross-section, the system is frozen in liquid nitrogen upon cutting and freeze-drying. A coating of 8 nm thick gold layer is deposited on the samples prior to imaging by using an SC7620 Polaron mini sputter coater (Quorum Technologies Ltd., Ashford, UK). For TEM imaging, freeze-dried samples are immersed in ethanol and placed on a copper mesh with an amorphous carbon membrane. After four hours of drying in a vacuum drier, samples were analyzed with FEI Talos F200X TEM (acceleration voltage of 200 kV). Furthermore, EDX is performed in STEM mode. For this purpose, a high-angle annular dark-field detector and a Super-X EDX system with four silicon drift detectors (SDDs) are applied.

To examine the surface topography of the samples, atomic force microscopy (AFM, Ntegra, NT-MDT), equipped with a silicon cantilever (NSG01, NT-MDT, tip radius 10nm) (HA-NC, NT-MDT,) is selected. Measurements are performed in a semi-contact mode, with a resonance frequency of 200 kHz and 500x500 points per image.

Dynamic light scattering (DLS) Zetasizer Nano ZS (Malvern, UK) is used to measure the hydrodynamic diameter of AgNCs. Measurements are performed on dispersions of 0.1% wt of AgNCs in water loaded into quartz micro cuvettes.

4.4. Chemical characterization

A Multiskan GO spectrophotometer (Thermo Scientific, USA) is used for the detection of ultraviolet-visible (UV-Vis) spectra, scanning in the range of 400-1000 nm every 5 nm.

FT-IR spectroscopy is used to characterize the functional groups of the hydrogel networks. FT-IR analyses are conducted in an attenuated total reflectance (ATR) mode with a Bruker Vertex70 FT-IR Spectrometer and carried out in the wavenumber range of 400-4000 cm^{-1} with a resolution of 2 cm^{-1} and 12 scans for each sample.

Commentato [2]: Details to be inserted

4.5. Nanomechanical characterization

AFM nanoindentation analysis is carried out to detect the Young's Modulus of the PAAm and PAAm/AgNCs hydrogels in a hydrated state. Measurements of surface mechanical properties are performed by testing the samples with AFM (Ntegra, NT-MDT) in an aqueous medium to prevent dehydration. A pre-calibrated CSG01 (NT-MDT) cantilever with a nominal tip radius

of 6 nm and a spring constant of 0.039 N/m is selected. Fifty nanoindentations from ten different surface areas are evaluated in each sample. The Young's moduli are then extracted and calculated by fitting the Hertz model to the loading curves acquired during the nanoindentation test.

4.6. Electrical characterization

Impedance measurements are performed using a Keysight E4990A impedance analyzer (Keysight Technologies). Electrodes are located between two conductive ITO glass slides (indium tin oxide coated, ITO, Sigma, 15–25 Ω/sq) connected with the impendence analyzer. The frequency range of 1 Hz to 10 kHz is selected for the detection of impedance values. The conductivity properties of polymers in film on glass were evaluated using a Keithley 2401 sourcemeter connected to an Alessi Instruments C4S four-point probe head (tips material: osmium; probe tip spacing: 1.6 mm; spring pressure: 40 g; probe tip diameter: 0.2 mm). The final results were calculated by averaging the data obtained by measuring the conductivity in ten different locations on five different films per sample.

4.7. *In vitro* biological response

4.7.1. Neural progenitor cell isolation and culture

NPCs are isolated from the sub-ventricular zone of 4-day-postnatal C57BL6 mice[27] and cultured according to an optimized protocol by Fiorelli et al.[28] Briefly, postnatal-day-4 mice are placed on ice and anesthetized. The mouse brain is extracted and the rostral Sub-Ventricular Zone is micro-dissected. After digestion in TripleX (Invitrogen) and 0.1% DNAseI at 37°C, the tissue is mechanically triturated by using glass Pasteur pipettes. Subsequently, the cell suspension is filtered through a 40 µm cell strainer (BD Falcon). 10^5 viable cells are placed in ultra-low attachment 6-well culture plates in presence of Dulbecco's Modified Eagle Medium/Nutrient Mixture F-12 (DMEM/F12) modified with 1:100 N2 (Gibco), 20 ng/ml of Epidermal Growth Factor (EGF, Peprotech), 20 ng/ml of Fibroblast growth factor 2 (FGF2, Peprotech), and 1:400 penicillin/streptomycin (Gibco). Within 7 days, progenitor neural cells crate floating neurospheres. Cell passaging has been carried out every 4-7 days, when cell density reaches 50 cells/µl.

4.7.2. Seeding of NPCs on PAAm/AgNCs hydrogels

In order to prepare the hydrogel samples for the seeding experiment, PAAm and PAAm/AgNCs hydrogels are placed in 4-well Petri dishes (Sigma, Poland) and sterilized under UV light for 30 minutes on each side. Samples are then incubated in a solution of 0.01% Poly-lysine for 12 hours at room temperature (RT), followed by the treatment with 0.001% Laminin for 2 hours at 37°C.

Subsequently, mature neurospheres with a diameter of 150 +/- 50 µm are manually selected and seeded on the hydrogels' surface. Samples are cultured at 37°C and 5% $CO_{2\ in}$ in a differentiation medium composed of Neurobasal A medium modified with 1:50 B27 (Gibco), and 1:200 penicillin/streptomycin. Medium has been changed every two days up to 10 days.

4.7.3. Immunohistochemical staining and imaging.

Hydrogels with seeded cells are fixed in 4% paraformaldehyde at each selected time point: 3 and 10 days of culture. Samples are washed in Phosphate Buffer Solution (PBS) and incubated for 30 minutes in a blocking solution of 0.4% Triton-X and 10% inactivated Goat Serum (Gibco) in PBS at RT. Chicken Anti-Map2 (Synaptic Systems) and mouse anti-GFAP (Millipore, clone GA5) primary antibodies have been diluted in 0.4% Triton-X with 2% Goat Serum in PBS in a dilution of 1:1000 and 1:500, respectively. Samples are incubated in the primary antibody solution overnight at 4°C. After washing, a secondary antibody solution is applied, and the hydrogels are incubated for 2 hours at 4°C. The secondary antibody solution is composed of goat anti-mouse Alexa 568 and goat anti-chicken Alexa 488 (Invitrogen) diluted 1:2000 in 0.4% Triton-X with 2% Goat Serum in PBS. Staining of nuclei is carried out by incubating the samples in a solution of 1:500 DAPI in PBS for 15 minutes. Immunohistochemical assays are imaged using a confocal microscope (Leica) using 20x objective lens, with a resolution of 1024×1024 pixels. Image quantification and analysis are performed using ImageJ National Institute of Health, USA).

4.8. *In vivo* experiments

4.8.1. Animals

15 young adult (3 to 6 months old) male c57BL/6 mice were used for this study. Mice were obtained from the Nencki Institute vivarium. Animals were housed in a controlled environment (21 ± 1° C, 40% humidity; lights off between 8:00 AM to 8:00 PM) in cages with 2-3 littermates before surgery and housed separated in the same environment post-surgery. Food and water were available *ad libitum*. The experimental protocols followed the European Communities Council Directive and the Animal Care Act (Poland) and were approved by local and national authorities.

4.8.2. Surgery

All surgeries were performed based on the protocols described previously [23,24]. Animals were anesthetized with isoflurane (1,5%, 0,5 l/m oxygen) and injected subcutaneously with Tolfedine (4 mg/kg), Butomidor (2 mg/kg) and Baytril (5 mg/kg). Four/Six regions of the skull were carefully marked using stereotactic coordinates with reference to Bregma (frontal: AP +2, ML +/-1.5 (motor); caudal: AP -1.5, ML +/-3.5 (somatosensory) or AP -3.5, ML +/-2.7 (visual)). The skull was thinned with a dental drill or trepan and removed. After stabilizing the surgical site with saline, PAAm/AgNCs- or PAAm-based systems were placed gently on the surface. As control conditions, Matrigel® (Sigma-Aldrich) was also tested using the same procedure; non-treated regions were also analyzed. For the purpose of chronic longitudinal experiments (histological and electrophysiological), electrodes were covered with an additional layer of soft medical-grade silicone which covered the skull and craniectomies with tested materials, and the skin was closed with surgical sutures/surgical skin glue. In the case of chronic *in vivo* recordings, silver ball electrodes were placed on the surface of tested materials. Electrodes, short connecting wires, and connector socket were covered and secured with dental acrylic.

4.8.3. Evaluation of biocompatibility

Histology. Mice were perfused transcardially with 4% paraformaldehyde. Brains were sliced coronally into 40 μm sections using Leica 1850 cryostat. Slices were permeabilized with 0.3% Triton X-100 (0.5% in the case of TMEM119 staining) and blocked for 4 hours in 5% Normal Goat Serum (NGS, Vector Laboratories, #S-1000). The following primary antibodies were used: rabbit polyclonal anti GFAP (1:100, Abcam #ab7260), rabbit polyclonal anti TMEM119 (1:200, Abcam #ab209064), mouse monoclonal anti TNF alpha (1:20, Abcam # ab1793), rabbit polyclonal anti Iba1 (1:500, GeneTex #GTX101495). TNF alpha and Iba1 were stained on the same slices, TMEM119 and GFAP were stained on separate but adjacent slices. Slices were washed 3 × 10 min in PBS and incubated for 2 h at RT with the following secondary antibodies: GFAP, Alexa Fluor 488 goat anti-rabbit (1:400, Abcam #ab150077), TMEM119, Alexa Fluor 568 goat anti-rabbit (1:400, Abcam #ab175471), TNF alpha, Alexa Fluor 568 goat anti-mouse (1:400, Abcam #ab175473), Iba1, Alexa Fluor 647 goat anti-rabbit (1:400, Abcam #ab150079). Lastly, preparations were washed in PBS 3 × 10 min and mounted on superfrost slides in Fluromount with DAPI (Invitrogen #00-4959-52).

Laser Scanning Microscopy. Sections were imaged using a Zeiss LSM 780 microscope (Carl Zeiss, Jena, Germany) with ZEN software. The following imaging settings were used: DAPI - excitation with diode laser (λex=405 nm), λ_{em}= 415-501 nm, BS 405; A488 - excitation with Argon laser (λex=488 nm), λ_{em}= 490-608 nm; A568 - excitation with DPSS diode (λex=561

nm), λ_{em}= 570-623 nm; A647 - excitation with HeNe laser (λex=633 nm), λ_{em}= 637-725 nm. For all Alexa probes BS 488/561/633 was used. Imaging was done over a Plan-Apochromat 20x/0.8 M27 objective lens, with a resolution of 1024×1024 pixels. Pinhole was adjusted to 1 AU for each fluorochrome. Stacks of images across the slice thickness were obtained with 1 µm z-increment. Quantitative analysis of the marker-positive cells was performed using ImageJ. Images were thresholded using a built-in algorithm (OTSU). Z projections were obtained and cells were counted manually by an investigator blind to the experimental condition. Cell counts were presented as the number of cells per mm^2.

4.8.4. ECoG recording and analysis

Silver ball electrodes with a diameter of 0,7 mm were created by heating the tip of 0.125 mm silver wire and soldering the end to a small electronic connector. For acute (non-survival) experiments, electrodes were fixed to a stereotaxic micromanipulator. This allowed lowering them onto tested materials placed on craniectomies and then rising them up to change the materials. Three to six material changes were performed and ECoG signal was consecutively recorded in each craniectomy. In the case of chronic recordings, implanted materials were tested in the same locations at chosen time points (immediately post-implantation, 1 week, 2 weeks, 3 weeks, and 6 weeks post-implantation).

Surgical level of Isoflurane anesthesia induced substantial depression of neuronal activity. Thus, after finalizing surgical procedures, for the recording session isoflurane flow was reduced as much as possible (to ~1%) to record evoked potentials, but was kept high enough to ensure animal comfort (i.e. slow breath rate, no muscle tension). Much lighter anesthesia was needed during chronic recording sessions, when no invasive procedures were performed, and the strongest responses were obtained in the first recording session post-implantation, when mice were recovering from anesthesia.

ECoG signal was amplified (x1000), filtered (0.1 Hz - 5 kHz, 8-channel Pyżanowski differential amplifier), digitized (10 kHz sampling rate, Power 1401 interface, Cambridge Electronic Design, UK, Spike2 software), and fed to a personal computer. Custom-written scripts were used for data acquisition and generation of TTL signals triggering sensory stimuli. Somatosensory responses were evoked by 0.15 mm movement of a piezoelectric slab attached to the whiskers. Stimuli were repeated with an interval randomly ranging between 3 and 5 seconds. Visual responses were evoked by a flash of white-light-emitting diodes (LEDs, (7600 cd/ m2 luminance, 2-ms duration) placed 10 cm in front of the mouse eyes.

Data processing was performed in Matlab (ver 2021b) with help of EEGlab[29] functions and custom-written scripts. Signal sweeps (-0.5 to 1.0 around each stimulus) were extracted, sweeps contaminated with artifacts were removed, and clean data were averaged to obtain evoked potentials (EP) - visual (VEP) and somatosensory (SEP). The magnitude of evoked response was estimated by calculating RMS of all values within post-stimulus window incorporating main EP waves (SEP: 5-100 ms; VEP: 40-400 ms; **Figure S8**).

4.9. Statistical analysis

Measurements have been carried out at least in triplicate, unless specified. Data are displayed as average values ± standard deviation. A one-way ANOVA statistic test is performed, and significant differences are shown when $p \leq 0.05$. More in details, statistically significant values are reported as $*p \leq 0.05$, $**p \leq 0.01$, $***p \leq 0.001$, and $****p \leq 0.0001$.

Supporting Information

Supporting Information is available from the Wiley Online Library or from the author.

Acknowledgments

This study was supported by the First TEAM grant number POIR.04.04.00-00-5ED7/18-00, which is conducted within the framework of the First TEAM programme of the Foundation for Polish Science (FNP) and co-financed by the European Union under the European Regional development Fund. C.R., P.N., and F.P. acknowledge the financial support from the Polish Ministry of Science and Higher Education through scholarships for outstanding young scientists. C.R. was partially supported by FNP. Figures 1, 4a, and 7a are created with Biorender; Figures 3f and 3g are partially created with Biorender.

Received: ((will be filled in by the editorial staff))
Revised: ((will be filled in by the editorial staff))
Published online: ((will be filled in by the editorial staff))

References

[1] M. Hauschild, G. H. Mulliken, I. Fineman, G. E. Loeb, R. A. Andersen, *Proc Natl Acad Sci USA* **2012**, *109*, 17075.

[2] C. Liang, Y. Liu, W. Lu, G. Tian, Q. Zhao, D. Yang, J. Sun, D. Qi, *Nanoscale* **2022**, *14*, 3346.

[3] A. Campbell, C. Wu, *Micromachines (Basel)* **2018**, *9*.

[4] K. J. Miller, D. Hermes, N. P. Staff, *Neurosurg. Focus* **2020**, *49*, E2.

[5] S.-H. Sunwoo, S. I. Han, H. Joo, G. D. Cha, D. Kim, S. H. Choi, T. Hyeon, D.-H. Kim, *Matter* **2020**, *3*, 1923.

[6] S. Guler, M. Dannhauer, B. Roig-Solvas, A. Gkogkidis, R. Macleod, T. Ball, J. G. Ojemann, D. H. Brooks, *Neuroimage* **2018**, *173*, 35.

[7] T. Zhou, G. Hong, T.-M. Fu, X. Yang, T. G. Schuhmann, R. D. Viveros, C. M. Lieber, *Proc Natl Acad Sci USA* **2017**, *114*, 5894.

[8] A. Ahnood, N. D. Truong, B. Fleiss, A. Nikpour, O. Kavehei, *Sens. Diagn.* **2022**, *1*, 245.

[9] S. Park, H. Yuk, R. Zhao, Y. S. Yim, E. W. Woldeghebriel, J. Kang, A. Canales, Y. Fink, G. B. Choi, X. Zhao, P. Anikeeva, *Nat. Commun.* **2021**, *12*, 3435.

[10] S. Zhao, P. Tseng, J. Grasman, Y. Wang, W. Li, B. Napier, B. Yavuz, Y. Chen, L. Howell, J. Rincon, F. G. Omenetto, D. L. Kaplan, *Adv. Mater.* **2018**, *30*, e1800598.

[11] D. Zhang, F. Di, Y. Zhu, Y. Xiao, J. Che, *J. Bioact. Compat. Polym.* **2015**, *30*, 600.

[12] P. Thoniyot, M. J. Tan, A. A. Karim, D. J. Young, X. J. Loh, *Adv Sci (Weinh)* **2015**, *2*, 1400010.

[13] J. Nam, H.-K. Lim, N. H. Kim, J. K. Park, E. S. Kang, Y.-T. Kim, C. Heo, O.-S. Lee, S.-G. Kim, W. S. Yun, M. Suh, Y. H. Kim, *ACS Nano* **2020**, *14*, 664.

[14] F. Chan, H. Syu, T. Wang, Z. Tang, C. Huang, J. Lee, T. Burnouf, S. Hu, P. Chen, W. Huang, *Adv. Mater. Interfaces* **2021**, *8*, 2100694.

[15] Y. Ohm, C. Pan, M. J. Ford, X. Huang, J. Liao, C. Majidi, *Nat. Electron.* **2021**, *4*, 185.

[16] K. Krukiewicz, J. Britton, D. Więcławska, M. Skorupa, J. Fernandez, J.-R. Sarasua, M. J. P. Biggs, *Sci. Rep.* **2021**, *11*, 1295.

[17] Y. Ziai, F. Petronella, C. Rinoldi, P. Nakielski, A. Zakrzewska, T. A. Kowalewski, W. Augustyniak, X. Li, A. Calogero, I. Sabała, B. Ding, L. De Sio, F. Pierini, *NPG Asia Mater.* **2022**, *14*, 18.

[18] A. Kim, W. B. Ng, W. Bernt, N.-J. Cho, *Sci. Rep.* **2019**, *9*, 2639.

[19] A. K. Gaharwar, N. A. Peppas, A. Khademhosseini, *Biotechnol. Bioeng.* **2014**, *111*, 441.

[20] T. Vignaud, H. Ennomani, M. Théry, *Methods Cell Biol.* **2014**, *120*, 93.

[21] S. C. P. Norris, J. Soto, A. M. Kasko, S. Li, *ACS Appl. Mater. Interfaces* **2021**, *13*, 5929.

[22] Y. Qin, C. Qiu, Y. Hu, S. Ge, J. Wang, Z. Jin, *ACS Appl. Mater. Interfaces* **2020**, *12*, 46609.

[23] R. Czajkowski, B. Jayaprakash, B. Wiltgen, T. Rogerson, M. C. Guzman-Karlsson, A. L. Barth, J. T. Trachtenberg, A. J. Silva, *Proc Natl Acad Sci USA* **2014**, *111*, 8661.

[24] K. Łukasiewicz, M. Robacha, Ł. Bożycki, K. Radwanska, R. Czajkowski, *J. Vis. Exp.* **2016**.

[25] A. Więckowska-Gacek, A. Mietelska-Porowska, M. Wydrych, U. Wojda, *Ageing Res. Rev.* **2021**, *70*, 101397.

[26] G. Olmos, J. Lladó, *Mediators Inflamm.* **2014**, *2014*, 861231.

[27] R. Fiorelli, K. Azim, B. Fischer, O. Raineteau, *Development* **2015**, *142*, 2109.

[28] R. Fiorelli, A. Cebrian-Silla, J.-M. Garcia-Verdugo, O. Raineteau, *Glia* **2013**, *61*, 2100.

[29] A. Delorme, S. Makeig, *J. Neurosci. Methods* **2004**, *134*, 9.

In this work, a biocompatible conductive nanostructured hydrogel-based neural biointerface has been designed and fabricated by adding Ag nanocubes into a PAAm hydrogel network. The final platform provides the incorporation of the hydrogel composite in a double-layered PDSM/soft skin adhesive silicon template for the stable long-term recording of neural signals *in vivo*.

C. Rinoldi, Y. Ziai, S. Zargarian, P. Nakielski, K. Zembrzycki, R. Fiorelli, M. Lanzi, A. Kostrzewska-Księżyk, R. Czajkowski, E. Kublik, L. Kaczmarek, F. Pierini*

In Vivo Chronic Brain Cortex Signal Recording Based on a Soft Conductive Hydrogel Biointerface